THE EFFECT OF GEOMETRICAL ELECTRICAL CABLE CONFIGURATIONS ON HEAT TRANSFER IN CABLE DUCTS

Kruger S.* and Pretorius L.**

*Author for correspondence
Department of Mechanical Engineering Science, University of Johannesburg
Auckland Park, Johannesburg, 2006,South Africa, E-mail: skruger@uj.ac.za
** Faculty of Engineering , the Built Environment and Information Technology, Department of Engineering and Technology Management, University of Pretoria ,South Africa. E-mail: Leon.Pretorius@up.ac.za

ABSTRACT

In this paper a numerical study of two-dimensional conjugate natural convection in square cavity containing heated cylinders and outer isothermal boundaries is performed. The cavity is designed to simulate an unfilled trough containing electrical cables. The purpose of this paper is to investigate the effect of geometrical arrangements of electrical cables in underground cable ducts on the heat transfer from the cables. The numerical investigation is performed using Computational Fluid Dynamics. Asymetric flow around the cables caused the temperature distributions around the cables for the different geometric arrangement to be dissimilar. The local Nusselt number around the cables was a function of the angle (θ), and the Nusselt number distributions vary for each cable and arrangement. The diagonal arrangement was found to be the least favourable, as this arrangement leads to higher temperatures in the cables compared to the vertical and horizontal arrangement.

INTRODUCTION

An important phase of the design of electrical power systems is the thermal analysis of the electrical cables. The current-carrying capability (ampacity) is directly influenced by the heat transfer through the cable components (the maximum permitted conductor temperature) and their surroundings [1]. Various types of cable installations are utilized in industry for example: directly buried, in duct banks, in backfills in filled or unfilled troughs and in casings to name a few [2]. When unfilled troughs are used, the cable circuits must frequently support high current ratings. Very often, the current carrying capability is limited by the ability of the conductor to dissipate the heat generated by the conductor into the trough. Electrical insulation deteriorates at an accelerated rate if the cables operate above a specified maximum allowable temperature [3]. Several cables are often placed inside troughs, and the heat transfer from the various cable arrangements in the cable troughs need to be investigated. The maximum transmitted power is limited by the maximum temperatures allowed for insulating materials.

Koch et al [4] compared buried Gas-Insulated transmission lines (GIL) with XLPE-cables for the same buried parameters. They found that GIL was the most reliable solution, and met the requirements better than the cable. The temperature at the GIL conductor remained below the limits, whereas the temperature of the cable was significantly higher compared to the GIL, leading to fast ageing.

Pilgram et al [5] investigated the rating of cables in unfilled surface troughs. It was found that the continuous rating could be increased by almost 28% when full natural ventilation is used in existing covered troughs. Lui et al [6] used the finite element method to investigate coupled conduction-convection in an underground rectangular duct containing three insulated cables. Some of the conclusions were that the centre cable had a higher temperature and lower Nusselt number compared to the side cables. It was also observed that the soil thermal conductivity had a significant effect on the local Nusselt number. Dvorsky et al [7] developed a new approach for the determination of temperature in electric conductors.

Natural convection has been the focus of numerous researchers due to its wide range of engineering applications. Applications range from nuclear reactors, aircraft fuselage, cooling of electronic components and underground electrical transmission cables. Often it is important that conduction and natural convection be taken into account simultaneously. A typical application of conjugate heat transfer with natural convection is unfilled troughs containing electrical cables.

Conjugate heat transfer has been investigated by various authors. Natural convection heat transfer for air from two vertically separated heated cylinders inside a rectangular enclosure with conducting vertical walls was investigated by Lacroix and Joyeux [8]. It was found that the Nusselt number along the vertical wall was a complex function of both the Rayleigh number and the dimensionless conductivity ratio. Heat transfer was found to be significantly influenced by the coupling effect between solid wall conduction and fluid convection. Sambamurthy et al [9] investigated laminar conjugate natural convection in horizontal annuli. They developed correlations as functions of Grashof number for different configurations, aspect ratios and thermal conductivity ratios. Conjugate natural convection heat transfer in an inclined square cavity containing a conducting block was investigated

by Das and Reddy [10]. They concluded that up to Ra = 10^3, conduction is the main mode of heat transfer. It was also found that a body with a higher conductivity ratio of solid to fluid can transfer more heat compared to a body with a low ratio beyond the critical point.

Conjugate heat transfer in eccentric annuli has been the focus of a number of studies. El-Shaarawi et al [11] studied geometry effects on the conjugate heat transfer. The same authors also investigated conjugate effects on steady, laminar natural convection heat transfer in vertical eccentric annuli [12].

An enclosure with a heat source of constant volumetric heat generation rate was investigated by Kuznetsov and Sheremet [13]. Results indicated with an increase in Grashof number, a steady thermal plume forms, and is also reflected by the cooling degree of the gas cavity.

The primary objective of this study is to provide information on the heat transfer characteristics for different geometrical placements of underground electrical cables in unfilled troughs The effect of natural convection heat transfer from three possible electrical cable arrangements will be investigated and some CFD results of the numerical analysis are presented in this paper.

NOMENCLATURE

dA	[-]	Surface Element
Gr^*	[-]	Modified Grashof Number
g	[m/s^2]	Gravitational Acceleration
k	[W/m°C]	Thermal Conductivity
$\bar{n}$	[-]	Vector Normal to Surface Element dA
Pr	[-]	Prandtl Number Pr = 0.7 for air
$\dot{q}^{"}$	[W/m^3]	Volumetric heat generation
Ra^*	[-]	Modified Rayleigh Number
S	[-]	Source term
$\bar{u}$	[-]	Velocity Vector
Greek Letters		
α	[m^2/s]	Thermal Diffusivity
β	[1/K]	Thermal Expansion Coefficient
Γ	[-]	Diffusion Coefficient
ϕ	[-]	Generalised Variable
ν	[m^2/s]	Kinematic Viscosity
ρ	[kg/m^3]	Density
Subscripts		
CV		Control Volume
D		Diameter

COMPUTATIONAL FLUID DYNAMICS

Introduction

The commercial CFD software StarCCM+ [14] was used for the numerical investigation in this study; this CFD software is based on the finite volume method. The dynamic behaviour of a fluid is governed by the following conservation laws of physics; conservation of mass, conservation of momentum and conservation of energy. The conservative form of all fluid flow equations can be written as:

$$\frac{d(\rho\phi)}{dt} + \mathrm{div}(\rho\phi\bar{u}) = \mathrm{div}(\Gamma \mathrm{grad}\,\phi) + S_\phi \qquad (1)$$

Where φ is a generalised variable. The first term is the rate of increase of φ of fluid element, the second the net rate of flow of φ out of the fluid element, the third term the rate of increase of φ due to diffusion, and the last term the rate of increase of φ due to sources [15]. Integrating Equation 1 over a three-dimensional control volume leads to:

$$\frac{d}{dt}\int_{CV}\rho\phi dV + \int_A \mathrm{div}(\rho\phi\bar{u})dV = \int_{CV}(\Gamma \mathrm{div}\,\phi)dV + \int_{CV} S_\phi dV \qquad (2)$$

Applying Gauss' theorem, equation 2 can be rewritten as follows:

$$\frac{d}{dt}\int_{CV}\rho\phi dV + \int_A \bar{n}.(\rho\phi\bar{u})dA = \int_A \bar{n}.(\Gamma \mathrm{grad}\,\phi)dA + \int_{CV} S_\phi dV \qquad (3)$$

The rate of change term is equal to zero in steady state problems, therefore the integrated form of the steady transport equation is given by:

$$\int_A \bar{n}.(\rho\phi\bar{u})dA = \int_A \bar{n}.(\Gamma \mathrm{grad}\,\phi)dA + \int_{CV} S_\phi dV \qquad (4)$$

It is nearly impossible to solve the previous mentioned equations using exact analytical numerical methods for general cases. The spatial discretization of the Navier-Stokes equations is the numerical approximation of the convective and viscous fluxes and the source term [16]. This aids in providing a road to approximate numerical solutions to the transport equations. The finite volume discretization method was used in this study, and is described in detail by for example Patankar [17] and Versteeg [15]. Natural convection was modelled by including the buoyancy source terms in the momentum equation by activating the gravity model in the software. In order to solve the conservation equations for mass, momentum and energy simultaneously using a time or pseudo-time marching approach, the coupled flow model was chosen as well as an extension of this model, the coupled energy equation. The formulation used by this model is particularly robust for solving flows with dominant source terms such as buoyancy [14]. In StarCCM+ turbulence is also simulated by solving the Reynolds-averaged governing equations for momentum, energy and scalar transport. Various turbulence models are available in StarCCM+; for this investigation the standard k-ε, low Reynolds number turbulence model was implemented. Conjugate heat transfer is solved in StarCCM+ by implicitly coupling the fluid and solid conservation law equations and solving them simultaneously [14].

NUMERICAL MODEL

In this investigation, a 600mm x 600mm trough containing 3 x 750 MCM aluminum cables are investigated. Three configurations are studied as shown in Figure 1.
:

1) Configuration 1: Horizontal cables
2) Configuration 2: Vertical cables
3) Configuration 3: Diagonal Cables

Figure 1: Arrangement of cables and numbers

Only a two dimensional analysis was conducted in this research. A polyhedral mesh was created, and the advancing layer mesher was activated as part of the CFD model of the cable trough system. In essence the discretized CFD geometry model is generated as follows: Layers of prismatic cells are generated around the surfaces of regions, and the mesher fills the remaining void with polyhedral cells. An advantage of this mesher is the ability to generate thicker, more uniform cell layers. To adequately capture heat transfer in the boundary layer a prism layer thickness of 3mm was specified, containing 5 prism layers. Volume sources were applied to the region around the cylinders to refine the mesh in these regions. The mesh parameters are shown in Table 1, and the mesh with the prism layer mesh are illustrated in Figure 2. The boundary conditions for the CFD model of the cable trough system are summarized in Table 2.

Table 1: Mesh Parameters

Property	Value
Base Size (m)	0.01
Number of Prism Layers	5
Prism Layer Stretching	1.5
Prism Layer Thickness (m)	0.003
Surface Growth Rate	1.3
Surface Size (Tet/Poly Density)	
Density	1.0
Growth Factor	1.0
Blending Factor	1.0
Volumetric Source	
Size Relative to Base (%)	10

To ensure that the number of prism layers specified was sufficient, the Wall Y+ values were monitored to ensure they are below 1.

Table 2: Boundary conditions

Boundary Name	Type	Physics
Vertical Walls	Wall	Isothermal
Horizontal Walls	Wall	Isothermal
Boundary of each cable	Contact Interface	Volumetric Heat Flux

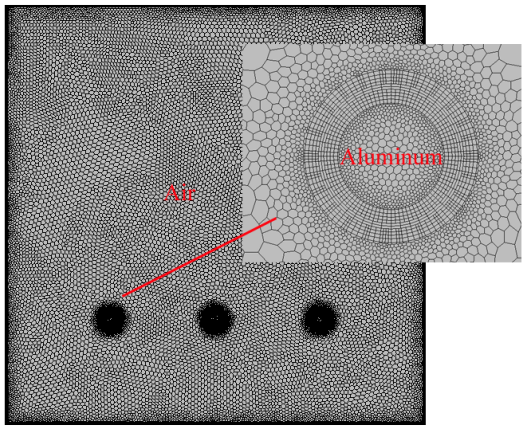

Figure 2: Typical mesh and prism layer mesh

Each electrical cable was specified as aluminum, with a thermal conductivity of 237W and at this stage of the research only a bare cable without insulation was modeled as the aim was only the comparison between geometrical variations. A volumetric heat generation due to the current flowing in the conductor was specified for each cable, based on the current and resistances specified for the cable in [18]. The heat flux was calculated to be $\dot{q} = 0.2 \times 181\,830 = 36\,366\ \text{W/m}^3$. At this stage of the research only 20% of the calculated or rated value was specified in the CFD model in the program as the focus here was only to compare the geometries for the same conditions in all the cables. The vertical walls and bottom walls of the cable trough were specified as isothermal with a temperature of 15°C, while the top wall of the trough was specified as 20°C to simulate in some sense the higher outside air as opposed to the cooler trough walls.. A mesh sensitivity analysis was conducted to ensure mesh independence. Taking simulation time into consideration, and the fact that the monitored temperature was not significantly influenced when decreasing the mesh size beyond 0.012m, it was decided to use a base size of 0.01m for all the simulations.

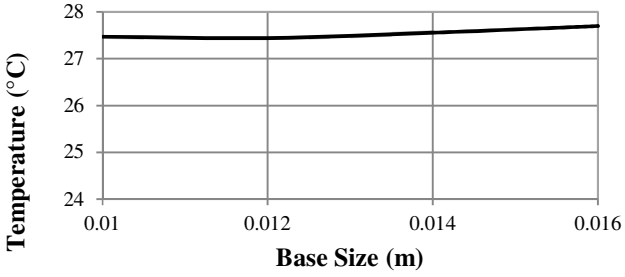

Figure 3: Results of mesh sensitivity analysis

If one considers only one cable with internal heat distribution and constant temperature, the modified Grashof number for this configuration based on the diameter is 1.69 x 10^6. In this current case the heat transfer effect is however distributed through three cables, equally spaced along the floor or wall of the cavity. If on this basis one then calculates the Grashof number on the height or length of the cavity, the Grashof number would be in the order of 10^9 which implies possible turbulent buoyancy driven flow. Therefore for this paper the CFD simulation is done for turbulent flow and the standard k-epsilon, low Reynolds turbulence model was used in the CFD model.

RESULTS

The two dimensional CFD results for the three configurations of electrical cables in a cable trough investigated numerically are given in the form of contour plots and graphs. The numerically simulated temperature and velocity contour plots for configuration 1 are shown in Figure 4. This plot indicates a large mushroom-shaped area of hot air in the upper half of the cavity, while the cavity is much cooler below the three cylinders due to the stagnant air trapped in this region. A temperature gradient is visible in the bottom half of vertical wall. The velocity contour plot indicates two large convective cells present in the cavity. Areas of high velocity in the top-half at the center of the cavity, against the top wall, and adjacent to the vertical walls is also noted. The hot air rises from each cable, and forms a single fluid stream moving towards the top of the cavity. At the top wall, the fluid stream splits into two, and moves down against the vertical walls. The fluid stream is cooled as it moves downward. From the two corners, the fluid stream once again moves toward the cables. The direction was deduced from vector plots not shown here.

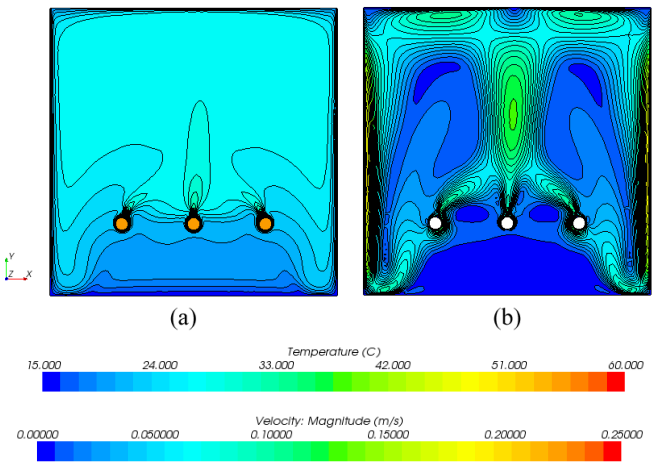

Figure 4: Temperature (a) and velocity (b) contour plot for Configuration 1

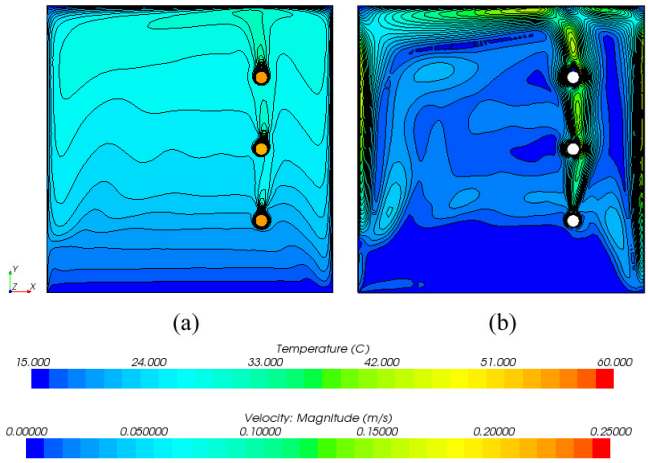

Figure 5: Temperature (a) and velocity (b) contour plot for Configuration 2

For configuration 2, the temperature contour plot shows a temperature stratified cavity, with the highest temperature noticed in the plume rising from the top cable. Two main convective cells form in the cavity. The warm air rises from the bottom cable, flows around the second and third cable and splits against the top wall of the cavity. The warm air then moves towards the left and right wall of the cavity respectively, and moves downward adjacent to the walls. The air on the left side of the cavity does not move all the way down towards corner as on the right side, but starts to move upward again at about a quarter of the cavity length from the bottom. The highest velocities are once again adjacent to the top and vertical walls of the cavity. A large stagnation area is present below the bottom cylinder in the bottom third of the cavity. Smaller stagnation areas are also present on top of cable 2 and 3 due to separation.

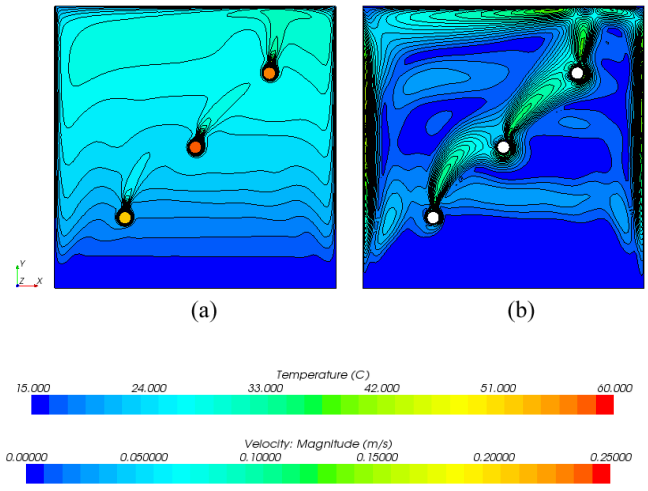

Figure 6: Temperature (a) and velocity (b) contour plot for Configuration 3

When the cables are arranged in a diagonal manner, the cavity is also characterized by layers of air (cold on the bottom, and gradually becomes warmer towards the top). This can be seen in Figure 6. The bottom cable is clearly at a lower temperature compared to the center and top cable. The velocity plot indicates air moving from cable to cable, and thereby creating a few distinct rotating cells in the cavity. Warm air once again reaches the top wall, and splits into two streams. Each stream moves toward the left and right wall respectively and downwards against the vertical walls. The bottom quarter of the cavity is relatively stagnant.

The temperature distribution at three different levels (0.15m, 0.3m and 0.45m) are shown in Figure 7 for configuration 1. The middle and top of the cavity display a similar homogenous temperature distribution, with temperature gradients against the vertical walls. At the bottom of the cavity (0.15m) the temperature distribution between the cables are lower (about 5°C) compared to the rest of the cavity, with a temperature gradient adjacent to the vertical walls. The temperature of the all three cables is approximately the same – 54°C. This can also be seen from Figure 8. Although the isotherms in the temperature contour plot in the temperature contour plot shown in Figure 4 seem to be symmetric about the center of the cavity, but the temperature distribution in Figure 8 indicates that this is not the case.

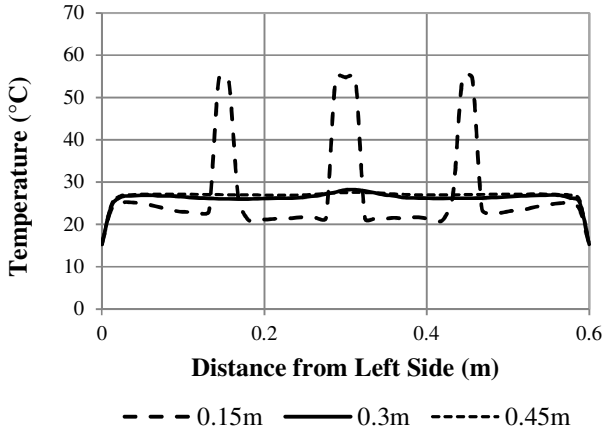

Figure 7: Temperature distribution at y = 0.15m, 0.3m, and 0.45m (Configuration 1)

Figure 9 shows the temperature distribution at three different levels for configuration 2. All three levels exhibit a homogenous temperature distribution, except close at the walls and in the vicinity of the cables where steep temperature gradients are noted.

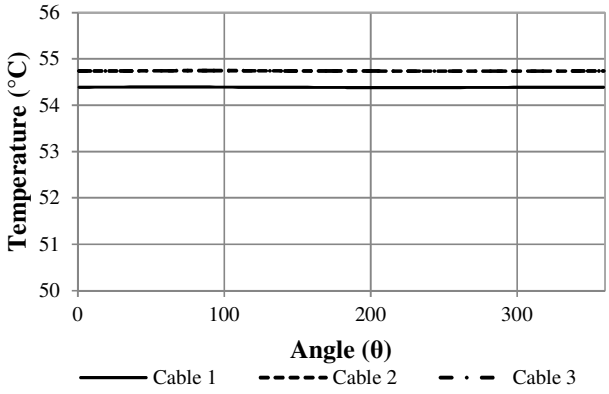

Figure 8: Temperature distribution around each cable (Configuration 1)

The bottom of the cavity is slightly cooler (approximately 21°C) compared to the centre (25°C) and top (27°C). Temperature gradients are visible in the vicinity of both vertical walls. The temperature for each cable is almost similar. Investigating the cable temperatures more closely, it can be seen that the second cable (centre) is the coolest. This is due to the plume of air rising from the first cable, assisting with the heat transfer. Most of the plume passes the cable on the right, while the air on the left of the cable is at a lower temperature. The top cable is at the highest temperature, due to the warm plume of the second cable moving around the cable.

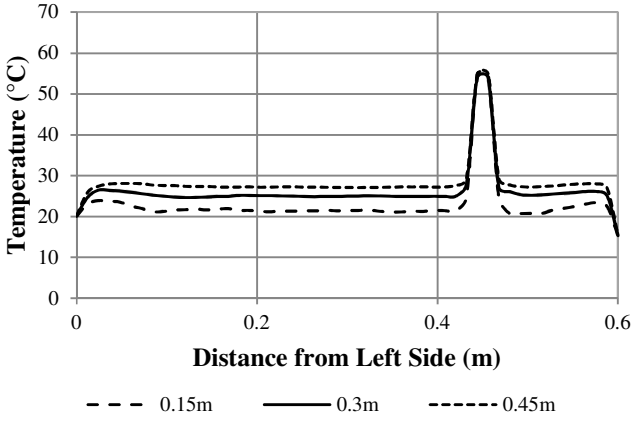

Figure 9: Temperature distribution at y = 0.15m, 0.3m, and 0.45m (Configuration 2)

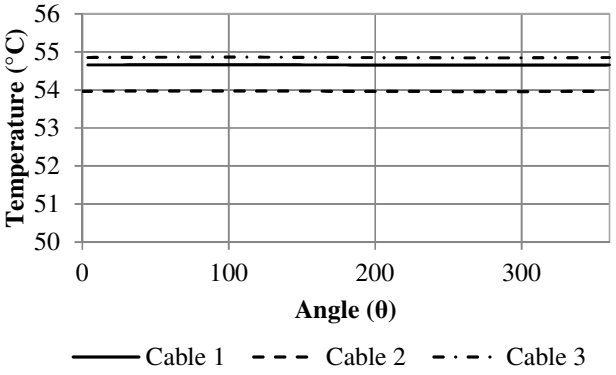

Figure 10: Temperature distribution around each cable (Configuration 2)

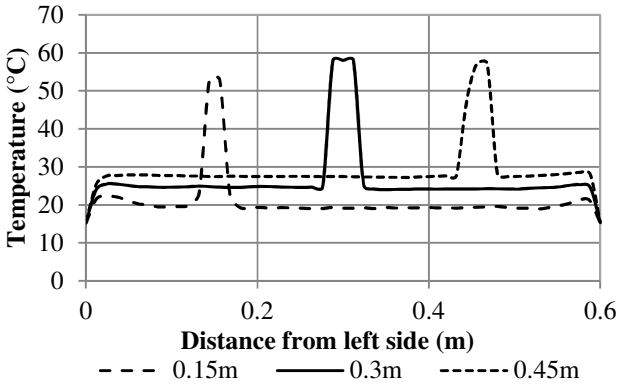

Figure 11: Temperature distribution at y = 0.15m, 0.3m, and 0.45m (Configuration 3)

The temperature distribution for the diagonal configuration is shown in Figure 11. Once again, at all three levels, the temperature distribution is mostly homogenous, with temperature gradients adjacent to the walls and close to the cables. From this plot it can be seen that the bottom cable (cable 1) is cooler (52.8°C) compared to cables 2 and 3 (approximately 58°C and 57°C respectively). Figure 12 shows a plot of the radial temperature distribution around each cable. The bottom cable is approximately 4°C cooler compared to cable 3. Cooler air circulates around the bottom cable, whereas the warmer plume from cable 1 accelerates to cable 2, and the plume from cable 2 rises towards cable 3. From the temperature distributions it can be seen that the diagonal arrangement is the least favourable, as this arrangement leads to higher temperatures in the cables compared to the vertical and horizontal arrangement.

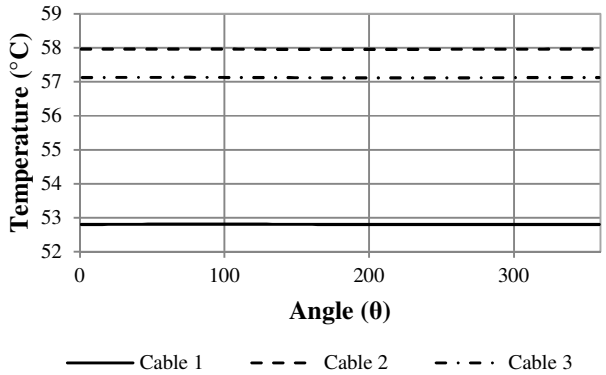

Figure 12: Temperature distribution around each cable (Configuration 3)

The Nusselt number distribution for each cable in configuration 1 is plotted in Figure 13. The Nusselt number varies from a minimum of 1.45(at θ = 66°) to a maximum of 7.8 (at about θ = 215°) for cable 1. The minimum Nusselt number for cable 2 and 3 are located at θ = 90 and 110° respectively. The convective heat transfer in this area is lower compared to the rest of the cable perimeter. Each minimum Nusselt number corresponds to a stagnation area adjacent to the cable in that area. Cable 2 exhibits a lower maximum Nusselt number (Nu = 6.7) compared to the other two cables.

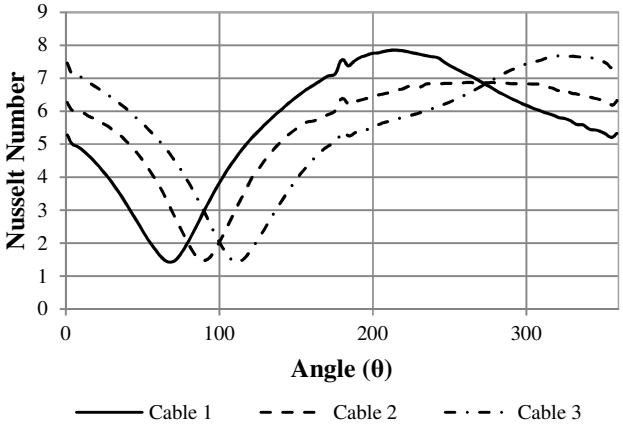

Figure 13: Nusselt number distribution for each cable (Configuration 1)

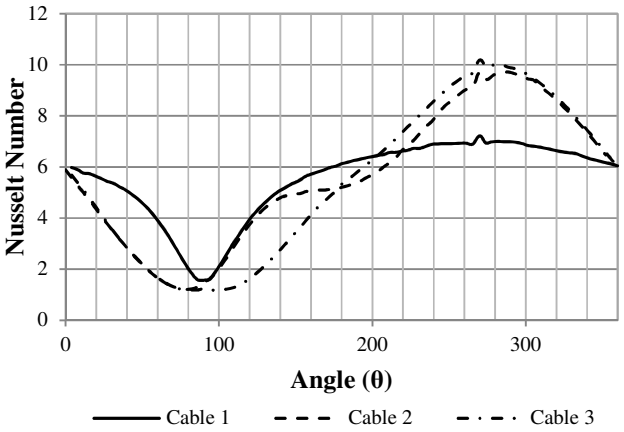

Figure 14: Nusselt number distribution for each cable (Configuration 2)

Figure 14 indicates the Nusselt number distribution for configuration 2. Cable 1 exhibits the lowest convective heat transfer, due the more stagnant flow area surrounding the bottom cable. A maximum Nusselt number in the region of 6.9 is observed. Cable 2 and 3 exhibit a higher maximum Nusselt number of almost 10. The convective heat transfer around cable 2 and 3 seem to be enhanced by the plume rising from the cable below. The Nusselt number for cable 2 and 3 is also similar between θ = 0° - 80°.

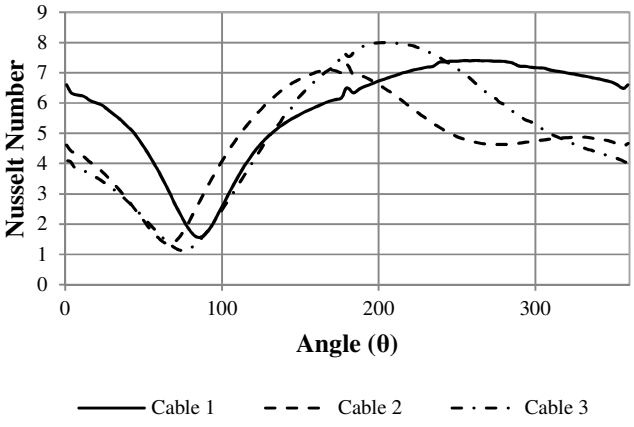

Figure 15: Nusselt number distribution for each cable (Configuration 3)

The Nusselt number distribution for the diagonal cable arrangement (configuration 3) is shown in Figure 15. The minimum Nusselt number (Nu = 1.6) is reached at θ = 90° for cable 1, whereas the minimum Nusselt numbers for cable 2 and 3 is at θ = 65° and θ = 75° respectively. The location of the minimum Nusselt number coincides with the position of a stagnation region on the boundary of each cable. Cable 3 exhibits a maximum Nusselt number at θ = 200° of 8. Once again, cable 2 and 3 hav the plume from the cable below circulating around it, therefore seeming to be enhancing the heat transfer. Cable 1 also has cool air flowing around it. The maximum Nusselt number for cable 1 is slightly lower, approximately 7.4. The difference in flow patterns around each cable leads to different Nusselt number distributions around the cable. This implies that the temperature gradients are not homogenous throughout the cable material, which may have an impact on the lifespan of the cable.

The CFD results presented in this paper are then based on the diameter of the cable for a specific cavity height H, and pitch distance between the cables, where H/D = 23.6 and P/D = 5.9. The modified Rayleigh number (based on the volumetric heat generation) was found to be 1.18 x 10^6 as defined as [19] in equation 1:

$$Ra_D^* = \frac{gBD^5\dot{q}}{\alpha k \nu} \tag{1}$$

And the modified Grashof number therefore 1.69 x 10^6 as defined by:

$$Gr_D^* = \frac{Ra_D^*}{\mathrm{Pr}} \tag{2}$$

The modified Rayleigh and Grashof numbers indicate laminar flow, but for the reason given earlier, the general flow in the numerical simulations were assumed to be turbulent.

CONCLUSION

Conjugate heat transfer in a cavity with isothermal walls and containing three heat-generating cylinders was numerically investigated in the present work. The cavity was designed to simulate an unfilled trough containing electrical cables. The main objective of this study was to investigate the effect of geometrical arrangements of electrical cables in underground cable ducts on the heat transfer around the cables. Due to asymetric flow around the cables, it was found that temperature distributions around the cables for the different geometric arrangement were not the same. The local Nusselt number was a function of the angle (θ), and the Nusselt number distributions vary for each cable and arrangement. The diagonal arrangement was found to be the least favourable, as this arrangement leads to higher temperatures in the cables compared to the vertical and horizontal arrangement. The results from this study indicate that different geometric arrangements influence the heat transfer around the cables, and may therefore have an impact on the ageing and lifespan of the cables.

Future work may include an investigation into the influence of laminar versus turbulent flow. The pitch versus diameter ratio can also be investigated further. It would also be beneficial to establish a Nusselt-Rayleigh relationship for the cavity containing the cables. Experimental flow visualization could also be attempted in future.

REFERENCES

[1] N. Kovac, N. Grulovic-Pavljanic and A. Kukavica, "Generated heat within power cable sheaths per unit time and volume," *Applied Thermal Engineering,* vol. 52, pp. 90-96, 2013.

[2] M. Terracciano, S. Purushothaman, de Leon, F and A. V. Farahani, "Thermal Analysis of Cables in Unfilled Troughs: Investigation of the IEC Standard and a Methodical Approach for Cable Rating," *IEEE Transactions on Power Delivery,* vol. 27, no. 3, pp. 1423 - 1431, 2012.

[3] G. M. Williams, P. L. Lewin and M. LeBlanc, "Accurate determination of ambient temperature at burial depth for high voltage cable ratings," in *IEEE International Symposium on Electrical Insulation*, Indianapolis, USA, 2004.

[4] H. Koch and A. Chakir, "Thermal Calculations For Buried Gas-Insulated Transmission Lines (GIL) and XLPE-Cable," *Power Engineering Society Winter Meeting,* pp. 857-862, 2001.

[5] J. A. Pilgrim, P. L. Lewin, S. T. Larsen, F. Waite and D. Payne, "Rating of Cables in Unfilled Surface Troughs," *IEEE Transactions on Power Delivery,* vol. 27, no. 2, 2012.

[6] Y. Lui, N. Phan-Thien, R. Kemp and X. Luo, "Coupled conduction-convection problem for an underground rectangular duct containing three insulated cables," *Numerical Heat Transfer,* vol. 31, pp. 411-431, 1997.

[7] K. Dvorsky, J. Gwinner and H. Liess, "A Fixed Point Approach to Stationary Heat Transfer in Electric Cables," *Mathematical Modelling and Analysis,* vol. 16, no. 2, pp. 286-303, 2011.

[8] M. Lacroix and A. Joyeux, "Coupling of wall conduction with natural convection from heated cylinders in a rectangular enclosure," *Int. Comm. Heat Mass Transfer,* vol. 23, no. 1, pp. 143-151, 1996.

[9] N. B. Sambamurthy, A. Shaija, G. S. Narasimham and M. V. Krishna Murthy, "Laminar conjugate natural convection in horizontal annuli," *International Journal of Heat and Fluid Flow,* vol. 29, pp. 1347-1359, 2008.

[10] M. K. Das and K. Saran Kumar Reddy, "Conjugate natural convection heat transfer in an inclined square cavity containing a conducting block," *International Journal of Heat and Mass Transfer,* vol. 49, pp. 4987-5000, 2006.

[11] M. A. El-Shaarawi, E. M. Mokheimer and A. Jamal, "Geometry effects on conjugate natural convection heat transfer in vertical eccentric annuli," *International Journal of Numerical Methods for Heat & Fluid Flow,* vol. 17, no. 5, pp. 461-493, 2007.

[12] M. A. I. El-Shaarawi, E. M. A. Mokheimer and A. Jamal, "Conjugate Effects on Steady Laminar Natural Convection Heat Transfer in Vertical Eccentric Annuli," *International Journal for Computational Methods in Engineering Science and Mechanics,* vol. 6, no. 4, pp. 235-250, 2005.

[13] G. V. Kuznetsov and M. A. Sheremet, "Conjugate natural convection in an enclosure with a heat source of constant heat transfer rate," *International Journal of Heat and Mass Transfer,* vol. 54, pp. 260-268, 2011.

[14] CD-Adapco, "StarCCM+ User Guide," CD-Adapco, 2012.

[15] H. K. Versteeg and W. Malalasekera, An introduction to Computational Fluid Dynamics, The Finite Volume Method,2nd Ed, England: Pearson Prentice Hall, 2007.

[16] J. Blazek, Computational Fluid Dynamics: Principles and Applications, Elsevier, 2005.

[17] S. V. Patankar, Numerical Fluid Flow and Heat Transfer, New York: Hemisphere, 1980.

[18] G. J. Anders, M. Coates and M. Chaaban, "Ampacity Calculations for Cables in Shallow Troughs," *IEEE Transactions on power delivery,* vol. 25, no. 4, pp. 2064-2072, 2010.

[19] M. A. Lamrani, T. Boulard, J. C. Roy and A. Jaffrin, "Airflows and Temperature Patterns induced in a Confined Greenhouse," *Journal of Agricultural Engineering Research,* vol. 78, no. 1, pp. 75-88, 2001.

[20] W. P. Jones and B. E. Launder, "The Prediction of Laminarization with a Two-Equation Model of Turbulence," *Int J or Heat and Mass Transfer,* vol. 15, pp. 30-314, 1972.